JOURNAL OF THERMOPHYSICS AND HEAT TRANSFER
Vol. 8, No. 4, Oct.–Dec. 1994

Proportional-Integral-Derivative-Controlled Numerical Model for the Programmable Multizone Furnace

C. H. Panzarella* and M. Kassemi†
NASA Lewis Research Center, Cleveland, Ohio 44135

This article presents a two-dimensional axisymmetric combined conduction and radiation model for the prototype of the programmable multizone furnace, which is under design at NASA Lewis Research Center. The actual furnace is intended for growing high-quality semiconductor crystals and performing other materials processing experiments in space. A novel feature of the model is a control algorithm that automatically adjusts the power in any number of independently controlled heaters to establish the desired sample temperatures during the numerical simulations. The control algorithm eliminates the need for numerous trial and error runs previously required to obtain the same results. The finite element code, FIDAP, was modified to directly incorporate the control algorithm. This algorithm, which presently uses proportional-integral-derivative (PID) control, and the associated heat transfer model are briefly discussed. Together, they have been used to predict the heater power distributions for a variety of furnace configurations and desired temperature profiles. Examples are included to demonstrate the effectiveness of the PID-controlled model in establishing isothermal, Bridgman, and other complicated temperature profiles in the sample. An example is also given to show how the algorithm can be used to change the desired profile with time according to a prescribed temperature-time evolution.

Nomenclature

A = surface area
C = specific heat
D = derivative coefficient
E = error between actual and set point temperature
F = matrix containing boundary condition information
F_{kj} = view factor between two surfaces k and j
h = heat transfer coefficient
I = integral coefficient
K = global system matrix containing conductivity information
K_{th} = thermal conductivity, scalar
L = heater wire length
M = matrix containing density and specific heat information
N = total number
$\boldsymbol{n}$ = unit normal vector
P = proportional coefficient
Q = heat source per unit volume
q = heat flux on a boundary
R = distance between radiation surfaces
T = temperature
t = time
$\boldsymbol{u}$ = vector of nodal temperatures
α = acceleration factor
δ_{jk} = Kronecker delta, 0 if $j \neq k$, 1 if $j = k$
ε = emissivity/error tolerance
θ = angle between connecting line and surface normal
ρ = density
σ = Boltzmann constant

Subscripts

A = actual
a = adjusted for the lead-in wires
air = pertaining to air
b = boundary
c = pertaining to four circular rings of heater wire
e = experimental measurement
f = pertaining to residual of solution
H = pertains to heaters
i = heater number/solution iteration number
j, k = radiation surface numbers/arbitrary indexes
m = pertaining to model
p = refers to constant pressure
r = radiation
S = setpoint
solid = pertaining to a solid material (insulator, heater, or sample)
t = total
u = pertaining to solution vector
∞ = ambient parameter

Received Feb. 4, 1993; revision received Jan. 8, 1994; accepted for publication April 11, 1994.

*NASA Research Assistant; currently Student, Physics and Applied Math Departments, University of Akron, Akron, OH.
†NASA/OAI Senior Research Scientist.

Introduction

THE programmable multizone furnace (PMZF) is a proposed design for a multipurpose furnace that can be easily configured for a number of different space experiments. One of the intended applications for the PMZF will be crystal growth in space, where the microgravity environment is thought to improve crystal quality. Although the furnace design is not complete, prototypes of the furnace have been built and tested in the Materials Processing Branch at NASA Lewis Research Center. These prototypes test the feasibility of the PMZF concept by examining the thermal characteristics of the design as well as predicting the overall power consumption of the furnace.

A major concern of the PMZF designers is to provide specific sample temperature profiles for the designated crystal growth experiments, with a stringent total power restriction of about 800 W. Therefore, accurate numerical predictions, especially with regard to power consumption, are extremely useful.

Most of the published work on numerical modeling of crystal growth furnaces have focused on Czochralski crystal growth systems[1-3] have reviewed a hierarchy of models for Czochralski growth. They have emphasized the need for an integrated analysis of the process that involves calculating temperature distributions in the melt, crystal, and the various components of the furnace. Published work on numerical

modeling of Bridgman furnaces in general and multizone furnaces in particular has been scarce. The most elaborate computational efforts have been due to Dupret et al.[4] and Crochet et al.[5] who incorporated the coupling between radiative, conductive, and convective heat transfer in their models. The latter investigators presented a finite element model for a Mellen furnace that closely resembles the furnace configuration here. Unfortunately, their work is not well suited for the PMZF project in two ways:

1) Since power was the input required by their model, they had to painstakingly adjust the power in their 26 heater zones to match the temperature distribution in the sample.

2) Although they were able to reproduce the temperature distribution in the sample, the resulting power predictions were off by a factor of 4.

These problems are addressed in this study by solving an inverse heat transfer problem in which the desired sample temperatures are the input and the heater powers are the output of the model. The inverse heat transfer problem is solved using a numerical proportional-integral-derivative (PID) algorithm. According to this method, the temperature field in the furnace is determined by obtaining numerical solutions to the transient energy equation using a finite element model of the furnace. The PID controller adjusts the heater powers in the furnace model based on the computed temperatures at each time step until the desired sample temperature profiles are achieved. In this way, the numerous trial and error steady-state runs previously required to obtain a specific sample temperature profile are replaced by one transient PID-controlled simulation. Thus, the user is conveniently removed from a tedious computational loop. This procedure is also useful for testing alternate control algorithms, which is an important design issue in advanced furnaces. The main objective of this article is to show that a control algorithm can be easily and efficiently incorporated into a numerical model to solve a class of inverse heat transfer problems that often occur in crystal growth furnace design. The concept, however, is not limited to crystal growth furnaces, but can be easily extended to other material preparation processes such as chemical vapor deposition or fiber growth.

A brief and general description of the furnace prototype will be given in the next section. This is followed by a discussion of the heat transfer mechanisms in the furnace and the associated numerical model. The model is used to produce isothermal, Bridgman, and other profiles in the sample for 1-, 2-, 4-, and 10-zone furnaces. These results are discussed and comparisons are made between the numerical predictions of total power consumption in the furnace and experimental measurements.

Theoretical Formulation

Physical Description of the PMZF Prototype

A typical configuration for a four-zone PMZF prototype, which is being developed in the Materials Processing Branch at NASA Lewis Research Center,[6] is shown in Fig. 1. The basic components of the prototype are the sample, the air gaps, the resistive heaters, the thermal insulation, and the aluminum cooling fins.

The sample is at the center of the furnace and has a cylindrical shape. In the cases studied in this article either boron nitride or gallium arsenide samples are considered. However, the boron nitride sample is the only one that was experimentally examined. There is an air gap between the sample and the heaters. Energy is exchanged between the heaters and the sample primarily by conduction through the air gap and radiation between the surfaces enclosing the air gap. The heaters are made of four windings of a multilayered resistive wire and two straight lead-in wires as indicated in Fig. 2. The heaters are connected to a power source via the lead-in wires. There is a small air gap between each heater coil and the surrounding insulating material, therefore, radiation exchange must be considered in those air gaps as well. The heaters are separated from each other by a layer of insulation as shown in Fig. 1. Therefore, each zone basically consists of a heater ring, an aluminum cooling fin, and a layer of insulation.

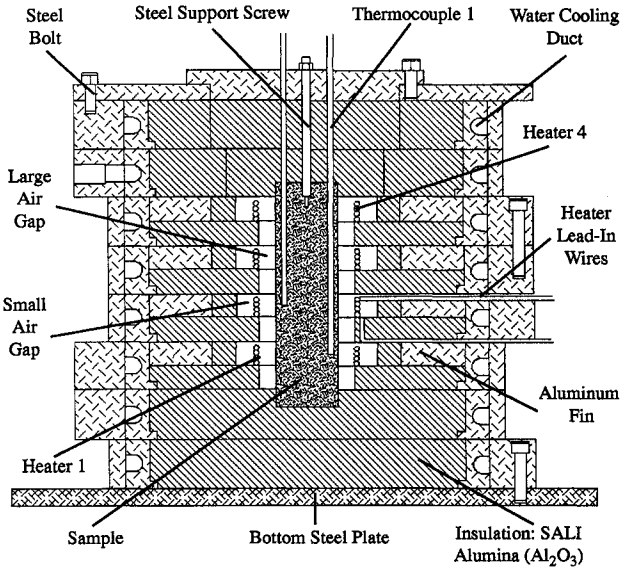

Fig. 1 Cross section of a four-zone PMZF.

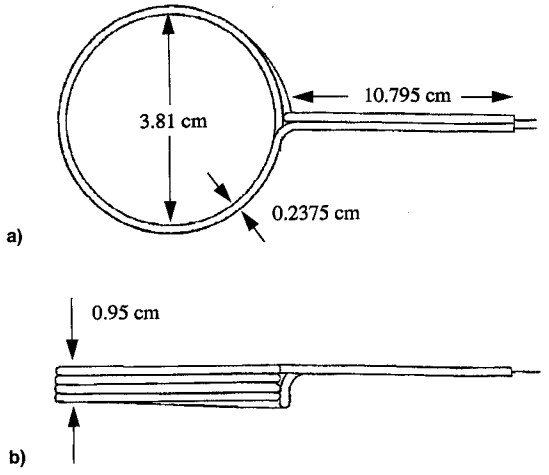

Fig. 2 Diagram of a typical heater used in the PMZF: a) top view and b) side view.

A distinguishing feature of this furnace design is the placement of aluminum fins around the heaters that extract heat radially from each zone. The amount of heat extraction in any zone can be varied by changing the size (the ratio of the outer to inner radius) of the corresponding aluminum fin. This provides great flexibility in achieving the desired temperature gradients in the sample. Finally, the outer aluminum shell that surrounds the entire furnace contains several water cooled ducts that can be used to increase the rate at which heat is extracted from the aluminum fins.

Governing Equations

The equations described below represent the heat transfer mechanism in a particular experimental furnace prototype. The sample as mentioned before is a solid rod, there is no crucible, and the sample is not melted in any of the cases examined. Therefore, effects that are related to phase change and convection are neglected, and heat transfer in the prototype is governed by the time-dependent conduction equation:

$$\rho C_p \frac{\partial T}{\partial t} = \nabla \cdot K_{th} \nabla T + Q \tag{1}$$

The source term Q in the above equation corresponds to the power input into the cylindrical heaters that, as will be described below, is controlled by the PID algorithm. Equation (1) is subject to heat flux boundary conditions at the outer boundaries

$$-K_{\text{th}}\frac{\partial T}{\partial n} = h(T_b - T_\infty) \tag{2a}$$

where h includes both convective and radiative contributions. Furthermore, at the surfaces between the air gaps and the solid materials (insulator, heaters, or sample) there is a balance between conductive and radiative heat fluxes expressed by

$$q_{\text{solid}} + q_{\text{air}} = q_r \tag{2b}$$

where q_{solid} and q_{air} represent the heat conducted to the surface through these materials, and q_r is the heat radiated from the boundary. To compute the radiation exchange, the internal boundaries are subdivided into a number of smaller surfaces, N_r. Assuming these arbitrary, small, computational surfaces are diffuse gray and have nearly uniform temperature and radiosity, the enclosure analysis[7] can be used to describe the net radiative heat flux of surface j denoted by q_j as ($1 < j < N_r$ and $1 < k < N_r$):

$$\sum_{j=1}^{N_r}\left[\frac{\delta_{kj}}{\varepsilon_j} - F_{kj}\frac{(1-\varepsilon_j)}{\varepsilon_j}\right]q_j = \sum_{j=1}^{N_r}(\delta_{kj} - F_{kj})\sigma T_j^4 \tag{3}$$

In the above formulation T_j is the temperature of each surface and the F_{kj} are the geometric view factors between radiation surfaces. The view factors, which represent the fraction of radiative energy leaving surface k that arrives at surface j, are calculated using a variation of the following general expression:

$$F_{kj} = \frac{1}{A_k}\int_{A_k}\int_{A_j}\frac{\cos\theta_k\cos\theta_j}{\pi R^2}\,dA_j\,dA_k \tag{4}$$

The view factors must satisfy the following energy conservation requirement:

$$\sum_{j=1}^{N_r} F_{kj} = 1 \tag{5}$$

Furnace Model

Since the furnace prototype is nearly symmetrical about its central axis, it is represented by a two-dimensional axisymmetric model as depicted by the coordinate system in Fig. 3. There is a source of circumferential asymmetry due to the heater lead-in wires as shown in Figs. 1 and 2. To avoid a full three-dimensional analysis, the lead-in wires were not included in the model, and each heater was approximated by a cylindrical ring. The lead-in wires are in direct contact with the aluminum cooling fins, and so the power dissipated by them is extracted from the furnace by the fins and carried out by the cooling fluid. Thus, neglecting the presence of the lead-in wires does not significantly affect the sample temperatures. The water-cooling channels, which were used to maintain a nearly constant temperature on the outside of the furnace, were not included in the model. Instead, Eq. (2a) was used to assign the outside surface temperature to the experimentally measured temperature at the boundaries that was nearly a uniform 27°C. This temperature was specified by using an artificially large heat transfer coefficient h with the ambient temperature T_∞, set to the experimentally measured surface temperature. In this way any loss of accuracy with regard to the power dissipated by the lead wires and carried out of the system by the cooling water was conveniently avoided.

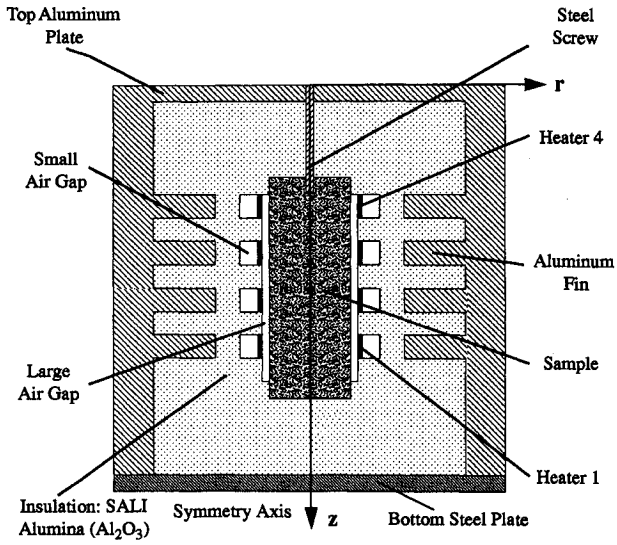

Fig. 3 Cross section of a four-zone PMZF model.

Control Algorithm

PID control is well suited for problems in which a single output is desired by controlling a single input parameter. In the furnace model, the controlled or "adjusted" quantity is the heater power, and the target quantity or output (also called the setpoint) is the desired temperature in the sample at a particular location. The power delivered to each heater is adjusted in order to reduce the error between the set-point temperature and the temperature computed by the numerical model at the desired location (referred to as an imaginary thermocouple). The power Q to each heater is adjusted using the following expression[8]:

$$Q = P\left[E + \left(\int E\,dt\right)\Big/ I + D\frac{d}{dt}E\right] \tag{6}$$

$$E(t) = T_S(t) - T_A(t) \tag{7}$$

In this way, the PID controller adjusts the power according to the proportion, time integral, and time derivative of the error. In the above equations, E is the error between the actual temperature T_A and the setpoint temperature T_S of the corresponding thermocouple. The three coefficients, P, I, and D, weight the effect of the proportional, integral, and derivative adjustments of the power, respectively. These coefficients must be determined by a trial and error process and may vary from case to case. The coefficients used in this study were chosen so that the steady-state temperatures would be attained rapidly and with minor temperature fluctuations. Expressions (6) and (7) are used to independently control each of the N_H heaters.

Numerical Implementation

The furnace model was developed using the finite element code FIDAP.[9] The temperature dependence of the material properties was incorporated in the numerical model by specifying the value of the conductivity, specific heat, and density of each material at specific temperatures. Linear interpolation from neighboring values was used to obtain the correct property values. Emissivity data for the solid materials bounding the radiation surfaces are difficult to obtain. In particular, the temperature dependence of the emissivities is not accurately known for many materials, so constant average values were used.

Nine-node isoparametric elements were used for all the results presented here. The average of the nine nodal temperatures in the "thermocouple" elements were compared to

the experimental temperature measurements made at the corresponding locations in the actual furnace.

Radiation view factors were computed between all the surface elements surrounding the air gaps. The number of radiation surfaces was increased until no significant difference was observed in the solution. FIDAP uses a version of the program FACET[10] to compute the radiation view factors between these surfaces. For a complicated geometry involving third surface shadowing such as the cylinder within a cylinder case examined here, the computations are more complicated and there might be small errors in the view factors. FIDAP provides a smoothing option that adjusts the view factors slightly (weighted by their magnitudes) so that their sum adds up to one as required by the relationship described in Eq. (5). Although this does not increase the accuracy of any one view factor, it ensures conservation of radiant energy. In this study, smoothing of the view factors was used even though its effect on the view factors was negligible.

Solution Procedure

Application of the Galerkin finite element procedure to the transient energy equation results in a set of equations that may be represented as

$$M(\bar{u})\frac{d\bar{u}}{dt} + K(\bar{u})\bar{u} = F \tag{8}$$

where $K(\bar{u})$ is a global system matrix containing information on the thermal conductivities as well as the coupling among the temperatures due to radiation as given by Eq. (3), $M(\bar{u})$ matrix that contains information on the density and specific heat of the materials, $\bar{u}$ is a global vector of unknown nodal temperatures, and F is a vector that includes the effect of the boundary conditions. Both $M(\bar{u})$ and $K(\bar{u})$ depend on temperature because the material properties are temperature-dependent. Therefore, these equations cannot be solved directly and an iterative technique is used.

A first-order implicit backward Euler scheme is used to approximate the continuous time derivative in Eq. (8). The result is an incremental procedure that advances the solution at discrete steps in time. A variable time stepping procedure is used that adjusts the time increment based on a local time truncation error at each step. This is more cost effective than a fixed time stepping approach because the solution may change dramatically during certain time periods and not much during others.

Iterative successive substitution is used to obtain the solution at each time step. The convergence of this scheme is slow (its convergence rate is asymptotically linear), but it provides the necessary robustness for problems involving nonlinearities associated with radiation. Two criteria are used to determine convergence at each time step: the relative error of the solution vector must be less than some specified tolerance ε_u and the other error tolerance ε_f is based on the residual vector of the solution, which must tend to zero as the iterates approach the true solution. Typical values for these tolerances are $\varepsilon_u = \varepsilon_f = 1.0 \times 10^{-3}$. The stability of the basic iterative procedure can often be improved by the use of an acceleration factor α ($0 < \alpha < 1$). At each time step, the next iterate in the successive substitution scheme u_{i+1}, is determined by

$$u_{i+1} + \alpha u_i + (1 - \alpha)\underline{u} \tag{9}$$

where u_i is the solution of the previous iteration, and $\underline{u}$ is the solution obtained by solving Eq. (8) with the coefficients evaluated at u_i. The acceleration factor is especially necessary when working with problems involving radiation. An acceleration factor of 0.7 was used in this study.

PID Control Algorithm

The PID algorithm adjusts a separate heat source Q_i for each heater in the model. At each time step of the transient solution of the energy equation, Q_i is adjusted using Eq. (6) with the error E_i determined using the temperatures obtained from the last converged time step. In the ideal situation this process continues until the thermocouples reach their setpoint temperatures, at which time the final heater powers are determined. An improper choice of the PID coefficients may result in a number of problems such as temperature oscillations about the set-point or the inability to achieve the desired sample temperature profile. For the present results only proportional and integral adjustments were used. The PID coefficients used in the model are different than those used in the experiment because they are controlling two different quantities. In the experiment, the PID controls the total power delivered to each heater. In the model, the PID adjusts the volumetric power density delivered to each model heater. In addition, the sampling times between the two cases are different as will be discussed later.

The successful implementation of a control algorithm in a numerical model requires a detailed knowledge of the structure of the numerical code and the characteristics of the transient solver. The interaction between the control algorithm and the solver is quite complicated. For example, the algorithm must allow for situations when the solution does not converge at a certain time level and the solver returns to the previous time level in order to proceed with a smaller time increment. The interested reader is referred to Panzarella and Kassemi[11] for a more complete description of the control algorithm together with flow charts and details of its incorporation into FIDAP.

Results and Discussion

The PID controlled simulations were used to determine the heater powers for a one-, two-, and four-zone furnace model. The thermocouple set-points for a particular four-zone case are presented in Fig. 4a. The resulting temperature profile along the center of the sample is also included in Fig. 4a, and the power distribution obtained by the PID algorithm is given in Fig. 4b. In this case the desired sample temperature was a uniform 900°C. In both the model and the experiment, steady-state temperatures of 900°C were achieved by starting from

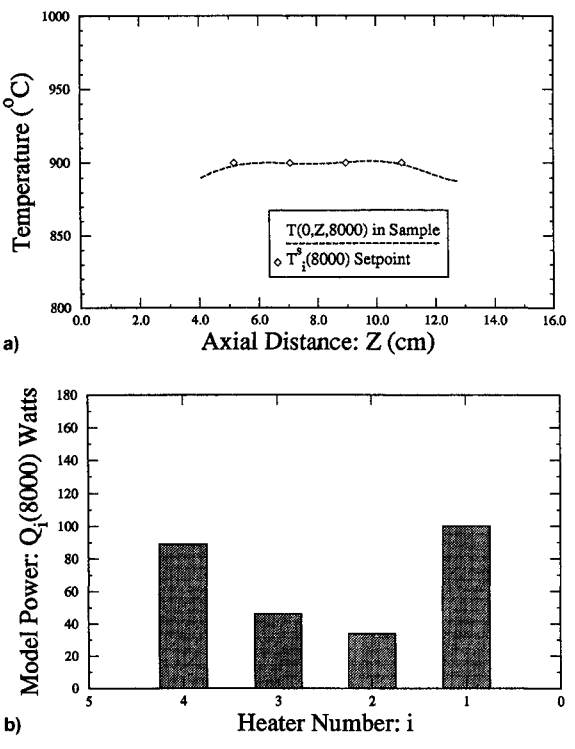

Fig. 4 a) Centerline sample temperature and b) heater powers for a four-zone furnace model, T_S = 900°C. Sample material was boron nitride. P = 0.35, I = 100, and D = 0.

Table 1 Temperature and power comparisons (boron nitride sample)

No. of zones	Cases	Sample temperature, °C				Power Q_e and Q_a, W			
		T4	T3	T2	T1	AP4	AP3	AP2	AP1
		a) T_S = 900°C							
One	Experiment	—	—	—	900	—	—	—	230
	Model	—	—	—	906	—	—	—	168
Two	Experiment	—	—	900	905	—	—	151	168
	Model	—	—	905	907	—	—	112	128
Four	Experiment	899	902	903	890	148	103	93	171
	Model	900	900	900	900	129	66	49	145
		b) T_S = 755°C							
One	Experiment	—	—	—	755	—	—	—	162
	Model	—	—	—	755	—	—	—	132
Two	Experiment	—	—	753	752	—	—	104	144
	Model	—	—	755	755	—	—	75	106
Four	Experiment	755	756	756	755	107	94	62	142
	Model	754	755	756	753	99	49	39	112

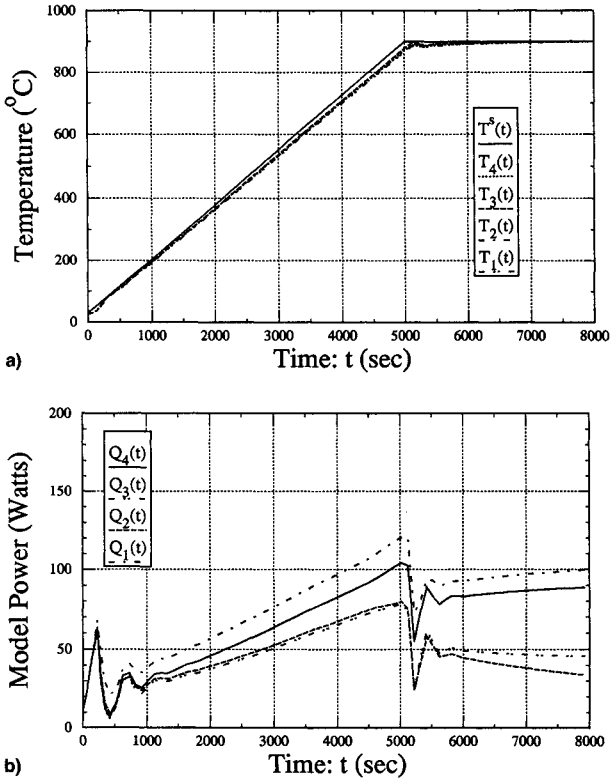

Fig. 5 a) Sample temperature and b) heater power histories for the four-zone furnace model, T_S = 900°C. Sample material was boron nitride. PID coefficients were P = 0.35, I = 100, and D = 0.

room temperature, 27°C, and ramping up at a rate of about 10.5°C/min as shown in Fig. 5. The PID coefficients were chosen by trial and error until the desired temperatures were achieved with minimal oscillation or overshoot. In this case, the coefficients P = 0.35 and I = 100 provided the desired response. The derivative was not used in this or any other case, and so its value is effectively D = 0.

The history of the temperatures and powers shown in Fig. 5 indicates an approach to steady state in about 8000 s. To maintain a constant temperature of 900°C, the end zones require more power than the intermediate zones. This is because they must compensate for heat loss through the top and bottom of the furnace in addition to the heat loss in the radial direction. Notice also that heater 1 requires more power than heater 4. This asymmetry is due to the extra extension of the air gap adjacent to heater 1, which introduces additional heat loss by radiation. This effect was also observed in the laboratory prototype and can be seen by examining the experimental powers of heaters 1 and 4 in Table 1.

Numerous experiments have been conducted to determine the total power required to maintain isothermal sample temperature profiles in one-, two-, and four-zone prototypes. This aspect is especially important for space applications because the final design of the furnace must operate within a total power requirement of approximately 800 W. PID-controlled simulations were used to predict the total power consumption in each case. A comparison between the numerically predicted powers and the experimental measurements is given in Table 1 for an average sample temperature of 900 and 755°C, respectively. This data is graphed in Fig. 6 as a function of average sample temperature. According to these results the model underpredicted the experimental powers by about 25%. This discrepancy did not change noticeably for different sample temperatures or as the number of heater zones increased. A numerical sensitivity analysis showed that the main source for the error is the thermal conductivity of the insulation material (SALI Alumina; Al_2O_3). The thermal conductivity data for the insulation used in the present simulations was obtained from the manufacturer's brochure, but little information was given with regard to the accuracy of the measurements. This conductivity is currently being measured to obtain more accurate property data for use in the model. Results of the sensitivity analysis and the conductivity measurements will be reported elsewhere.[12]

The power dissipated by the lead-in wires must be taken into consideration when comparing model and experimental results. The model power determined by the PID controller is adjusted by adding to it the fraction of power assumed to be dissipated by the lead-in wires. This fraction is determined by assuming the power is evenly dissipated along the total length of heater wire. The adjusted model power Q_a is related to the model power Q_m by the following expression:

$$Q_a = Q_m \times (L_t/L_c) \tag{10}$$

where L_t is the total length of heater wire in the furnace, and L_c is the length of the four circular coils of heater wire. For the current heater design, L_t/L_c is about 1.45, and so Q_m was increased by about 45% to obtain Q_a. Q_a was the value used in comparisons with experimental powers. With this relationship it is assumed that 69% of the total experimental power

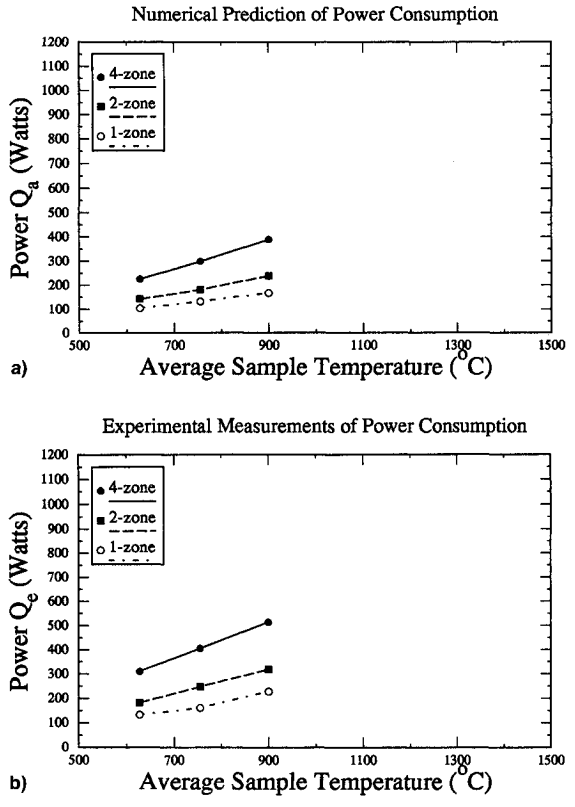

Fig. 6 Power consumption as a function of average sample temperature: a) numerical predictions and b) experimental results. The sample material was boron nitride.

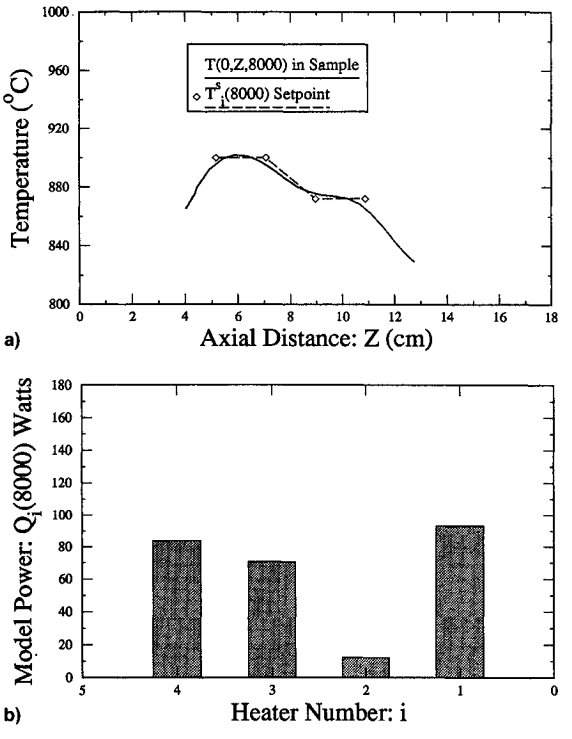

Fig. 7 a) Centerline sample temperatures and b) heater powers for a four-zone furnace model with Bridgman temperature profile. Specified temperature gradient between thermocouples 2 and 3 was 15°C/cm. P = 0.35, I = 100, and D = 0. Sample material was gallium arsenide.

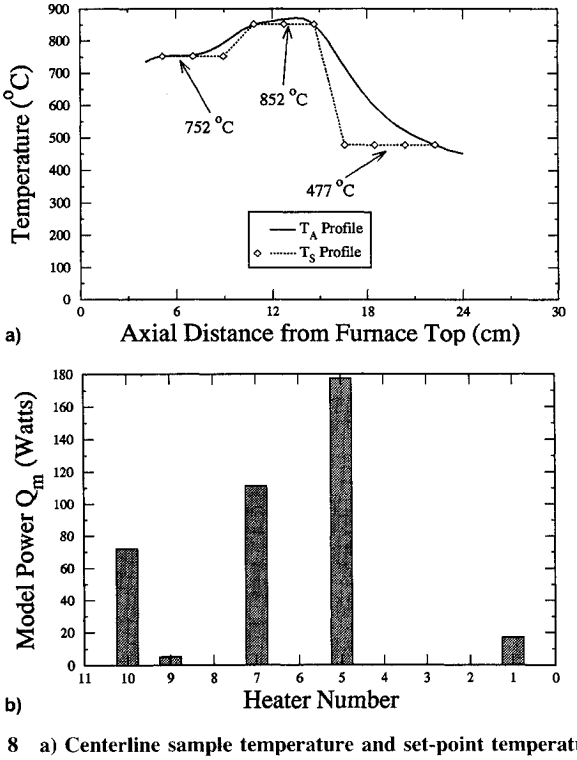

Fig. 8 a) Centerline sample temperature and set-point temperature profiles and b) heater powers for a 10-zone furnace model. P = 0.20, I = 800, and D = 0. Sample material was gallium arsenide.

Q_e is dissipated by the inner heater coils. The remaining 31%, which is dissipated by the lead-in wires, is assumed to be extracted by the aluminum cooling fins and removed from the system by the circulating water. Since, in this study, experimentally measured temperatures were prescribed at the furnace boundaries, only that percentage of the power dissipated by the inner heater coils can significantly affect the sample temperature predictions.

A typical Bridgman temperature profile was established in the sample for a four-zone furnace model using the same PID coefficients as in the isothermal case. A temperature gradient of about 15°C/cm was maintained between thermocouples 2–3 in the sample. The resulting temperature profile along the symmetry axis of the sample and the final PID determined powers per zone for this profile are presented in Fig. 7. The end zone powers (heaters 1 and 4) were quite similar to those of the constant sample temperature case, but heater 3 required more power, and heater 2 required less power than in that case. It is interesting that the total power for both cases was about the same; 269 W for the isothermal sample temperature, and 260 W for the Bridgman temperature profile. The average temperature of the sample in the Bridgman case was slightly lower than that in the isothermal case and probably explains the lower total power. Although not rigorously examined, it is probably reasonable to conclude from the above data that the total power required by the furnace is a function of the average sample temperature and is nearly independent of the particular temperature profile as long as the gradients are reasonably small compared to the average temperature levels. The distribution of the power among the various heaters, however, varies for different temperature profiles.

Often in crystal growth more complicated sample profiles are desired. An example with two different temperature gradients is shown in Fig. 8a. PID-controlled simulations of a 10-zone furnace model were used to determine the heater powers necessary to bring the sample temperature as close as possible to the desired profile. The resulting sample temperature profile and the PID-determined heater powers are shown in Figs. 8a and 8b, respectively. Heaters 5 and 7 need large powers to maintain thermocouples 5 and 7 at the required temperature of 850°C, whereas thermocouple 6 receives sufficient heat from heaters 5 and 7 to maintain (or exceed) this temperature. Therefore, no additional heat is required from heater 6 and it reduces its power until it shuts off (zero power).

The PID controller would need to request negative power (heat sinks) from the heater 6 and others to achieve the profile as specified. Such a situation is physically impossible, and so the PID controller simply shuts off the heater (specifies zero power) when negative heater power is requested. A similar situation occurs for the other neighboring thermocouples (thermocouples 2, 3, 4, 8, and almost 9) whose temperatures maintained or exceeded their set-point solely by the heat from heaters 5 and 7 and the end heaters 1 and 10, which must supply additional heat to account for top and bottom heat loss. This phenomenon is also observed experimentally when steep gradients are required by the user. It is also highly undesirable because when a heater in a given zone shuts off, it simply implies that the furnace cannot accommodate the required gradient with its current design and has to be reconfigured to provide more heat loss from the shut-off zones. Thus, the large errors between the sample temperature and the set-point temperature at certain thermocouple locations (notably at thermocouples 2, 3, and 4) are due to the specified temperature gradient and not to any defect in the model or PID controller. The model exactly fulfills its required task by indicating that this gradient is too steep to be achieved with the present design.

In view of the previous results, further investigation was carried out to determine the approximate maximum temperature gradient that can be maintained between adjacent thermocouples. This was done by lowering the cold end temperature until one of the heaters shut off. It appears that a maximum gradient of about 20°C/cm is possible for this sample material and furnace configuration.

In addition to determining the powers necessary to achieve a certain steady-state sample temperature profile, the PID algorithm can also be used to change a desired profile and the resulting sample temperatures with time. The process is illustrated using a two-zone furnace model. The set-point temperature of thermocouple 2 is maintained at 900°C while the set-point temperature of the other thermocouple is decreased

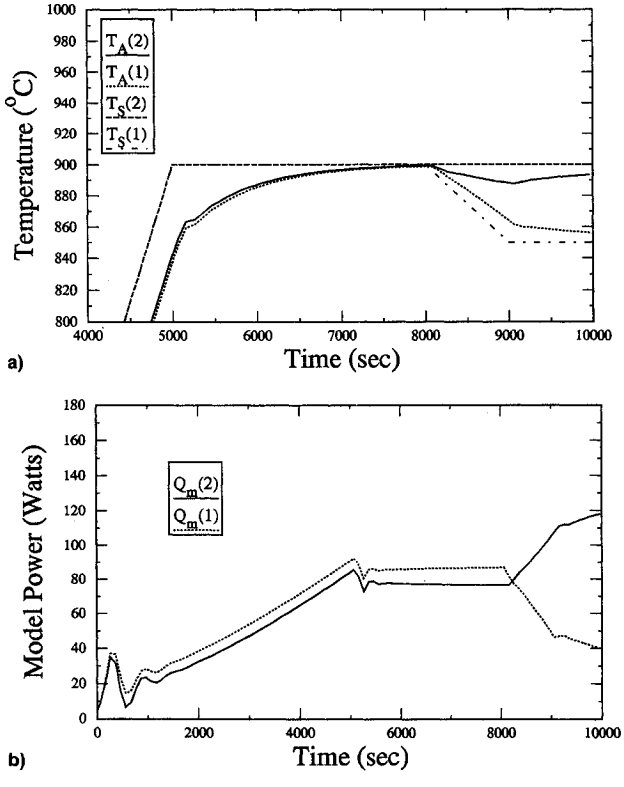

Fig. 9 a) Sample temperature and b) heater power histories for a two-zone furnace model with time-dependent set-point temperature. P = 0.15, I = 700, and D = 0. Maximum time step size: 100 s. Sample material was gallium arsenide.

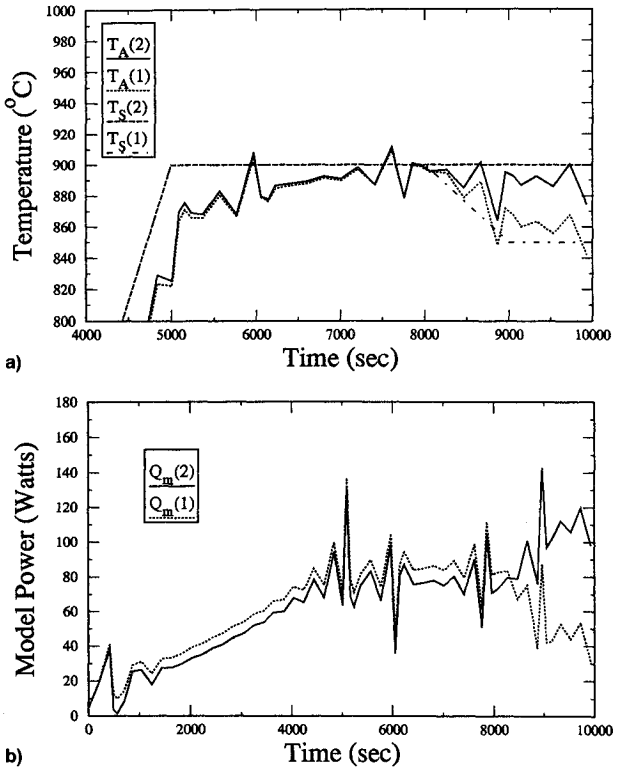

Fig. 10 a) Sample temperature and b) heater power histories for a two-zone furnace model with time-dependent set-point temperature. P = 0.15, I = 700, and D = 0. Maximum time step size: 200 s. Sample material was gallium arsenide.

linearly to 850°C. The time response of the thermocouple temperatures and heater powers are included in Figs. 9a and 9b, respectively. Although, it appears that the temperatures approach their setpoint, there is lag between the time at which a particular temperature is requested and the time at which the imaginary thermocouple attains this temperature. The coefficients were changed but the thermocouples still responded slowly. This lag is partly due to factors such as the mass or thermal inertia of the sample and partly because a better control strategy that takes into account the inherent coupling between the zones might be required for a faster response. The algorithm can be easily modified to incorporate a more sophisticated control technique.

One important distinction between the operation of the PID controller in the furnace model and in an actual furnace is that a controller used in an actual furnace is free to measure the temperatures at any time (limited only by the sampling rate of the electronic equipment). The numerical model, however, solves the transient energy equation at discrete time steps. Temperatures are only determined at these time intervals and are not available at intermediate times. Of course, the time steps could be chosen so that they match the sampling rate of temperatures in the real furnace, but this would be inefficient. The extensive computational time and memory storage requirement would make such a task impractical. In this study as mentioned before, time steps appropriate for an efficient solution of the transient problem were chosen by the transient solver. However, a maximum size for the time steps was specified to ensure an adequate sampling rate for the controller. If the time steps become too large, the response of the controller becomes erratic even though the solution is well converged at every time step. This is indicated in Fig. 10 where it is clear that a time step of 200 s produces an oscillatory response in both the power and the temperature histories, even though the temperatures are converged at each time step. This is expected since the large time steps reduce the sampling rate of the PID controller. When the sampling rate is too low, by the time the temperature information is

passed to the controller, the temperatures have changed considerably. The PID controller then makes a large adjustment in the heater power to counteract this response. This results in another drastic change in the temperatures, this time in the opposite direction and causes a periodic fluctuation in the power.

Conclusions

A general control algorithm was developed and incorporated in a combined conductive and radiative numerical model for a multizone furnace prototype. The algorithm used a PID control scheme, but can also use a multivariable, or other more advanced control strategies. The following conclusions can be made:

1) The numerical model agrees to within about 25% of experimental measurements of total power consumption with further improvements anticipated when the thermophysical and radiation properties are more accurately determined.

2) The PID algorithm can be used to determine the heater power distribution needed to produce a desired temperature profile in the sample of the furnace model. This process was carried out successfully for isothermal, Bridgman, and other complicated profiles.

3) It is possible to use the PID control algorithm to change a sample profile over time as was illustrated using a two-zone example. The process could be extended to furnace models with more zones, and could be used to translate the gradient along the sample as is done in actual solidification experiments. Further research is currently in progress in this area.

4) The control algorithm and the model can be used together as a design tool for engineers to test various design or control ideas.

5) The implementation of the PID controller in the model reduces the computational time for achieving a certain sample profile by replacing numerous trial and error steady-state runs with a single, PID controlled, transient simulation.

Acknowledgments

This work would not have been possible without the valuable input and guidance from the PMZF design team headed by Barry Licht and Cathy Krolikowski. We also want to gratefully acknowledge the important initial guidance provided by William Arnold with regard to the PID controller and the substantial help provided by Ron Gaug and Dave Thompson in system related and postprocessing issues.

References

[1]Bornside, D. E., Kinney, T. A., and Brown, R. A., "Finite Element/Newton Method for the Analysis of Czochralski Crystal Growth with Diffuse-Gray Radiative Heat Transfer," *International Journal for Numerical Methods in Engineering*, Vol. 30, 1990, pp. 133–154.

[2]Atherton, L. J., Derby, J. J., and Brown, R. A., "Radiative Heat Exchange in Czochralski Crystal Growth," *Journal of Crystal Growth*, Vol. 84, 1987, pp. 57–78.

[3]Brown, R. A., Kinney T. A., Sackinger, P. A., and Bornside, D. E., "Toward an Integrated Analysis of Czochralski Growth," *Journal of Crystal Growth*, Vol. 97, 1989, pp. 99–115.

[4]Dupret, F., Nicodéme, P., Ryckmans, Y., Wouters, P., and Crochet, M. J., "Global Modelling of Heat Transfer in Crystal Growth Furnaces," *International Journal of Heat and Mass Transfer*, Vol. 33, No. 9, 1990, pp. 1849–1871.

[5]Crochet, M. J., Dupret, F., and Ryckmans, Y., "Numerical Simulation of Crystal Growth in a Vertical Bridgman Furnace," *Journal of Crystal Growth*, Vol. 97, 1989, pp. 173–185.

[6]Licht, B. W., and Krolikowski, C. R., "Programmable Multizone Furnace," NASA Headquarters Code S. N. Rept., March 1991.

[7]Siegel, R., and Howell, J. R., *Thermal Radiation Heat Transfer*, 2nd ed., McGraw-Hill, New York, 1981, pp. 233–280.

[8]Eckman, D. P., *Automatic Process Control*, Wiley, New York, 1958, pp. 59–77.

[9]Engelman, M., *FIDAP Revision 5.04 Theoretical Manual*, Fluid Dynamics International, Evanston, IL, 1991.

[10]Shapiro, A. B., "FACET—A Radiation View Factor Computer Code for Axisymmetric, 2D Planar, and 3D Geometries with Shadowing," Lawrence Livermore Lab., UCID-19887, Livermore, CA, 1983.

[11]Panzarella, C. H., and Kassemi, M., "A Numerical Model Including a PID Control of a Multizone Crystal Growth Furnace," Micro/Macro Scale Phenomena in Solidification, American Society of Mechanical Engineers, HTD-Vol. 218, 1992, pp. 127–139.

[12]Kassemi, M., Panzarella, C. H., Desto-Sidik, K. E., Krolikowski, C. R., and Licht, B. W., "A Numerical-Experimental Study of the Programmable Multi-Zone Furnace (PMZF)," AIAA Paper 92-0691, 1992.